LAMINATE STIFFNESS TAILORING FOR IMPROVED BUCKLING PERFORMANCE

C. B. York[1]

[1] Singapore Institute of Technology, 10 Dover Drive, Singapore 138683

Christopher.York@singaporetech.edu.sg

www.singaporetech.edu.sg/directory/faculty/christopher-bronn-york

ABSTRACT

This article presents an algorithm to tailor bending stiffness properties for double angle-ply laminates. A database of orthotropic double angle-ply laminates is derived for non-crimp fabric configurations, highlighting the severity of this manufacturing constraint compared to the use of single unidirectional layers. The significance of the new algorithm is demonstrated through the development of a range of new laminate designs, all with matched isotropic bending stiffness properties, allowing the isolated effects of axial stiffness to be studied, in this case to improve the critical length at which the transition from local to overall mode instability occurs in thin walled columns. Many of the non-crimp fabric designs can be tapered in thickness, through ply terminations, without introducing undesirable thermo-mechanical coupling behaviour. These configurations can now be matched to either bending or extensional stiffness of equivalent balanced and symmetric laminate designs, which are shown to occupy only specific, ply number dependent regions within the design space. This is demonstrated for typical aircraft components, to identify configurations with improved buckling performance.

KEYWORDS

Double angle-ply laminates, Standard-ply laminates, Buckling, Stiffness matching, Lamination parameters, Taper.

1 INTRODUCTION

The use of advanced tailoring strategies to introduce specific mechanical and/or thermal behaviour into a laminated composite component continues to evolve, particularly with the introduction of Thin-ply or Spread-Tow technologies, such as C-Ply^{TM} (with a range of lamina areal weights down to as little as 50g/m^2), which offer significant benefits over conventional laminated materials (with lamina areal weights above 250g/m^2), by bringing design flexibilities found only in traditionally thick laminate construction into the thin laminate domain.

Manufacturers in the aerospace sector are considering the possibility of moving away from standard symmetric laminates, or so-called 'black metal' designs, but need further evidence that aero-elastically tailored composite materials can: produce weight savings; introduce aerodynamic efficiencies and/or reduce manufacturing time without incurring cost penalties.

Certainly, a two-fold increase in deposition rate is possible using non-crimp fabric (NCF) architectures, compared with automatic fibre placement (AFP) of unidirectional (UD) material to achieve a 'black metal' design. NCF designs allow angle plies to be deposited in a single axis pass, instead of the requirement for multiple passes in an off-axis direction to deposit a single layer of angle-ply material.

The continuing requirement for more efficient manufacturing of composite structures has inspired research into a broad range of bi-angle NCF architectures. Indeed, a recent study on repeating (r) bi-angle $[\theta/0]_{rT}$ NCF designs [1], has now led to commercially available forms [2]. However, the resulting unbalanced, non-symmetric laminate architecture, not only leads to mechanical (Extension-Shearing and Bending-Twisting) coupling but also to undesirable thermal warping; effects which dissipate only as the number of repeats (r) becomes very large.

More recent research in this area provides compelling evidence for ease of manufacture and improved performance in the relative in-plane strength [3,4] between standard-ply laminates (or classic quads) and double angle-ply laminates (or Double-Double designs), with non-standard angles. A technique for extensional stiffness matching between standard and double angle-ply laminates [5, 6] also permits like-with-like comparisons, based on ply percentages commonly used in the design

process for aircraft components. However, little consideration has previously been given to bending stiffness [7], which has a significant influence on buckling performance.

Stiffness tailoring of double angle-ply laminates has been considered previously [8], but was limited to the development of isotropy in either extensional or bending stiffness properties. The study used a double angle-ply design, which was derived from a fully uncoupled anti-symmetric laminate [9], formed from a combination of two symmetric sub-laminates [10]. Whilst isotropic laminates are of limited importance in the design of aircraft structural components, they do offer an important benchmark against which specific design performance indices can be measured. For instance, it is now well understood that a weight reduction can be achieved simply through the adoption of carbon-fibre reinforced plastics (CFRP), as a replacement for traditional aluminium alloys, but perhaps less well understood is the fact that when the laminate has isotropy in bending, together with matching thickness, the local plate buckling performance remains virtually unchanged. This is due to the fact that Graphite/Epoxy T300/5208 material has equivalent isotropic properties of E_{Iso} = 69.7 GPa, shear modulus G_{Iso} = 26.8 GPa and Poisson ratio ν_{12} = 0.3, see Table 1, which are virtually identical to the properties of aluminium alloys. Indeed, a hybrid laminate consisting of CFRP and aluminium layers would constitute an optimum fibre metal laminate (FML) in terms of stiffness compatibility, if not for the risk of galvanic corrosion [11].

In this article, a general approach to bending stiffness tailoring for double angle-ply laminates is presented. It exploits a new laminate database containing all possible solutions with up to 24 plies; chosen because practical designs for fully isotropic laminates will be shown to exist for this specific ply number grouping, using either standard or double angle-ply architectures.

New bending stiffness design charts, which map directly to buckling performance charts for infinitely long plates, are developed for all double angle-ply solutions.

Finally, design examples demonstrating the influence of extensional stiffness on buckling performance of classical thin walled Z-section columns with matched bending isotropy; such designs show an increase in effective length before the transition from local to overall buckling.

2 STIFFNESS TAILORING

Extensional stiffness is readily calculated for any laminate configuration by simply observing the proportion of ply angles, or ply percentages [6] in each of the four principal directions. In other words, the stacking sequence does not need to be defined, *a priori*. Bending stiffness on the other hand requires a knowledge of the specific stacking sequences that eliminate all undesirable coupling properties. Balanced and symmetric designs remain pervasive in aircraft composite design for the simple reason that symmetry guarantees the elimination of thermal warping distortion during high temperature curing. However, symmetry does not guarantee the elimination of *Bending-Twisting* coupling, which continues to be ignored, even when the detrimental effect on compression buckling strength is pertinent to the conclusions drawn about such as design.

A new database of double angle-ply laminate configurations, which eliminate specific mechanical coupling characteristics, are derived for non-crimp fabric (NCF) architectures as well as uni-directional (UD) solutions, i.e., solutions that are not constrained to specific NCF architectures. These configurations are used in conjunction with a new stiffness matching approach to obtain tailored laminate designs with specific bending stiffness properties. This permits performance and design choice comparisons between standard symmetric laminate configurations, to which design heuristics have been applied, and the new stiffness matched double angle-ply configuration. Tapered thickness, through ply terminations adds further design constraints to the laminate tailoring process and therefore listings of compatible tapered designs are also derived. These tapered solutions avoid the introduction of undesirable coupling characteristics.

2.1 Database of standard symmetric laminate configurations

A database of design information for fully uncoupled symmetric laminates with up to $n = 21$ plies is summarized in Fig. 1 and Table 2. These are also known as the classic quads, and are taken from a much larger database of predominantly non-symmetric designs [12] from which symmetric designs have been extracted, and to which the 10% rule, limiting the minimum number of plies in each of the

four principal orientations, and a ply contiguity constraint, limiting the maximum number of adjacent plies with identical orientation to 3, have both been applied.

In the original derivation of the database [12], all stacking sequences were developed with a single outer surface angle ply, as is common design practice, to improve damage tolerance, and which also served to eliminate the possibility of generating cross-ply only designs. Designs that represent merely a switch in the sign of the ply angles are not unique, hence the stacking sequences were originally listed in symbolic form (○, +, – and ●), to provide the designer with complete freedom to choose both the sign and the value of the ply angles. In the current article the symbols are assumed to represent standard angles 0, +45, -45 and 90°. The complete database of stacking sequences and corresponding lamination parameters is provided in Appendix 1 - Balanced and Symmetric Standard-Ply Designs.

The 39 points on Fig. 1(a) represent the lamination parameters for extensional stiffness. They are unique to a single ply number grouping (n), except for the 14- and 21-ply configurations, which share a common lamination parameter point. This results in a total of 41 distinct groups of fully uncoupled laminates, each with matching extensional stiffness. They represent a total of 527 designs, of which 507 are unique designs; the remainder share common lamination parameters. The designs fall within ply number groupings n = 12, 14, 16 – 21 plies. There are 566 unique designs if the contiguity factor constraint is relaxed.

Examples of the unique lamination parameter coordinates in Fig. 1(a) are presented in Table 2. These points represent stacking sequences from within one symmetric half of the design space ($\xi_1 \geq 0$). The remaining points in the design space are obtained by switching 0 and 90° plies in the stacking sequences. The examples given in Table 2(a) were chosen because they represent solutions with the highest increase in compression buckling strength above the equivalent isotropic design, expressed as a percentage. The list is very different if the results are representative of the highest shear buckling strength, as the list Table 2(b) demonstrates. The reasoning behind this is apparent from buckling design charts presented later in this article.

Ply percentages for standard-ply laminates are superimposed on the lamination parameter design space of Fig. 1(a), which include the in-plane lamination parameters (ξ_1, ξ_2) for typical aircraft components: Spar (0, -0.6), Skin (0.32, 0.12) and Stiffener (0.5, 0.4). These lamination parameters correspond, respectively, to the following ply percentages for 0°, ±45° and 90° ply orientations: Spar (10/80/10), Skin (44/44/12) and Stiffener (60/30/10). Tables 3 and 4, list the symmetric laminates most closely matching typical Skin and Spar properties, respectively. There are no solutions for a typical Stiffener component, with coordinate (ξ_1, ξ_2) = (0.5, 0.4) on Fig. 1(a). This requires a symmetric design with either a higher ply number grouping $n > 21$, or a symmetric design in which *Bending-Twisting* coupling is present. These results demonstrate the severe limitations imposed by the balanced and symmetric laminate design rule. The limitations related to design selection and also buckling performance above the so called black metal design, particularly the skin panels designs of Tables 3. All other designs within this specific range of balanced and symmetric designs possess *Bending-Twisting* coupling, which can result in up to a 10% reduction buckling strength [14-16].

2.2 Conversion from standard symmetric laminate configurations to double angle-ply designs

The database of fully uncoupled laminates with up to $n = 21$ plies [12] was again filtered to establish a list of designs that are readily converted to double angle-ply configurations. This requires a specific set of matching non-dimensional parameters. The development and use of these non-dimensional parameters is demonstrated by way of an example for a 16-ply laminate stacking sequence $[+/\bigcirc/\bullet/-_2/\bullet/\bigcirc/+/-/\bullet/\bigcirc/+_2/\bigcirc/\bullet/-]_T$, using the procedure set out in Table 5. Note that this design is not symmetric. Indeed, it can be described as having an anti-symmetric angle-ply sub-sequence together with a cross-symmetric cross-ply sub-sequence.

The first two columns of Table 5 provide the ply number and respective orientation, whilst subsequent columns illustrate the summations, for each ply orientation, of $(z_k - z_{k-1})$, $(z_k^2 - z_{k-1}^2)$ and $(z_k^3 - z_{k-1}^3)$, which relate to necessary calculations for the **A**, **B** and **D** stiffness matrices, respectively. Here, the interface distance, z, of the k^{th} layer from the laminate mid-plane, is expressed in terms of ply

thickness t; assumed to be unit value. The non-dimensional parameters arising from the tabular summations are treated as follows.

For the extension stiffness matrix, **A**, the number of (0° = 90°) cross plies, $n_{\circ} = n_{\bullet}$ ($_{A}\Sigma_{\circ} = {}_{A}\Sigma_{\bullet}$) = 4, the number of angle plies $n_{-} = n_{+}$ ($_{A}\Sigma_{-} = {}_{A}\Sigma_{+}$) = 4. The coupling stiffness matrix summations confirm that the contributions from all ply angles are zero for this laminate, hence **B** = **0**. For the bending stiffness matrix, **D**, the bending stiffness parameter for (0° and 90°) cross plies $\zeta_{\circ} = \zeta_{\bullet}$ (= 4 × $_{D}\Sigma_{\circ}$ = 4 × 244 = $_{D}\Sigma_{\bullet}$ = 4 × 244) = 976, whilst the bending stiffness parameter for angle plies $\zeta_{+} = \zeta_{-}$ (4 × $_{D}\Sigma_{+}$ = 4 × 268 = 4 × $_{D}\Sigma_{-}$ = 4 × 268) = 1072. A factor of 4 is applied to the bending stiffness parameters to balance the relationship between extensional and bending stiffness parameters such that n^3 (= $n_{\circ}$+ $n_{\bullet}$ + n_{-} + n_{+})^3 = 16^3 = ζ (= $\zeta_{\circ}$+ $\zeta_{\bullet}$ + ζ_{-} + ζ_{+}) = 4096.

Due to the balanced nature of this laminate configuration, the angle ply sub-sequence parameters may be conveniently combined to a single parameter: $n_{+} + n_{-} = n_{\pm\psi}$. The same reasoning may be applied to the cross ply sub-sequence parameter, which can be extended to replacing the cross plies with a second set of angle plies $n_{\circ} = n_{\bullet} = n_{\pm\phi}$.

The conversion to double angle-ply designs therefore requires an equal number of cross-ply layers as well as angle-ply layers:

$$\begin{aligned} n_{\circ} = n_{\bullet} &\rightarrow n_{\pm\phi} = n_{\circ} + n_{\bullet} \\ n_{+} = n_{-} &\rightarrow n_{\pm\psi} = n_{+} + n_{-} \end{aligned} \tag{1}$$

together with equalities in their bending stiffness contributions:

$$\begin{aligned} \zeta_{\circ} = \zeta_{\bullet} &\rightarrow \zeta_{\pm\phi} = \zeta_{\circ} + \zeta_{\bullet} \\ \zeta_{+} = \zeta_{-} &\rightarrow \zeta_{\pm\psi} = \zeta_{+} + \zeta_{-} \end{aligned} \tag{2}$$

The laminate stacking sequence $[+/\bigcirc/\bullet/-_2/\bullet/\bigcirc/+/-/\bullet/\bigcirc/+_2/\bigcirc/\bullet/-]_T$, developed in the above example, can therefore be recast in double angle-ply form as $[+\psi/+\phi/-\phi/-\psi_2/-\phi/+\phi/+\psi/-\psi/-\phi/+\phi/+\psi_2/+\phi/-\phi/-\psi]_T$. Note however that this configuration is representative of a class of double angle-ply design that cannot generally be manufactured using balanced NCF layers consisting of $\underline{+\phi/-\phi}$ and $\underline{+\psi/-\psi}$ pairs. Such double angle-ply designs are therefore referred to as UD designs and the number of solutions for each ply number grouping is reported in Table 6 as Uncoupled UD. Non-crimp fabrics are addressed in the following section.

All double angle-ply designs derived in this way will retain their fully uncoupled behaviour. The complete database for these UD designs, with up to $n = 24$ plies, is provided in Appendix 2: Double Angle-Ply Designs Derived from Standard-Ply Designs. Stacking sequences and their corresponding non-dimensional parameters, $n_{\pm\psi}$, $n_{\pm\phi}$, $\zeta_{\pm\psi}$ and $\zeta_{\pm\phi}$, are grouped by ply number (n) and matching extensional stiffness parameters $n_{\pm\psi}$, $n_{\pm\phi}$ and ordered by ascending bending stiffness parameter $\zeta_{\pm\psi}$. Note that $(\zeta_{\pm\psi} + \zeta_{\pm\phi}) = \zeta = n^3$.

The common feature relating all standard and double angle-ply designs in this article is that they are decoupled, i.e. $B_{ij} = 0$; hence in-plane and out-of-plane behaviour are independent and can therefore be treated separately. The constitutive relations, involving force and moment resultants and their corresponding strains and curvatures, simplify as follows:

$$\begin{Bmatrix} N_x \\ N_y \\ N_{xy} \end{Bmatrix} = \begin{bmatrix} A_{11} & A_{12} & 0 \\ & A_{22} & 0 \\ \text{Sym.} & & A_{66} \end{bmatrix} \begin{Bmatrix} \varepsilon_x \\ \varepsilon_y \\ \gamma_{xy} \end{Bmatrix}$$

$$\begin{Bmatrix} M_x \\ M_y \\ M_{xy} \end{Bmatrix} = \begin{bmatrix} D_{11} & D_{12} & 0 \\ & D_{22} & 0 \\ \text{Sym.} & & D_{66} \end{bmatrix} \begin{Bmatrix} \kappa_x \\ \kappa_y \\ \kappa_{xy} \end{Bmatrix} \qquad (3)$$

The non-dimensional parameters are used to calculate the elements of the extensional, **A**, and bending, **D**, stiffness matrices from the following relations:

$$A_{ij} = \{n_{\pm\psi}Q'_{ij,\psi} + n_{\pm\phi}Q'_{ij,\phi}\} \times t$$
$$D_{ij} = \{\zeta_{\pm\psi}Q'_{ij,\psi} + \zeta_{\pm\phi}Q'_{ij,\phi}\} \times t^3/12 \quad (4)$$

where the transformed reduced stiffness terms in Eqs. (4) are given by:

$$Q'_{11} = Q_{11}\cos^4\theta + 2(Q_{12} + 2Q_{66})\cos^2\theta\sin^2\theta + Q_{22}\sin^4\theta$$
$$Q'_{12} = Q'_{21} = (Q_{11} + Q_{22} - 4Q_{66})\cos^2\theta\sin^2\theta + Q_{12}(\cos^4\theta + \sin^4\theta)$$
$$Q'_{16} = Q'_{61} = \{(Q_{11} - Q_{12} - 2Q_{66})\cos^2\theta + (Q_{12} - Q_{22} + 2Q_{66})\sin^2\theta\}\cos\theta\sin\theta$$
$$Q'_{22} = Q_{11}\sin^4\theta + 2(Q_{12} + 2Q_{66})\cos^2\theta\sin^2\theta + Q_{22}\cos^4\theta \quad (5)$$
$$Q'_{26} = Q'_{62} = \{(Q_{11} - Q_{12} - 2Q_{66})\sin^2\theta + (Q_{12} - Q_{22} + 2Q_{66})\cos^2\theta\}\cos\theta\sin\theta$$
$$Q'_{66} = (Q_{11} + Q_{22} - 2Q_{12} - 2Q_{66})\cos^2\theta\sin^2\theta + Q_{66}(\cos^4\theta + \sin^4\theta)$$

where θ corresponds to ply orientations ψ or ϕ, and the reduced stiffness terms are given by:

$$Q_{11} = E_1/(1 - \nu_{12}\nu_{21})$$
$$Q_{12} = \nu_{12}E_2/(1 - \nu_{12}\nu_{21}) = \nu_{21}E_1/(1 - \nu_{12}\nu_{21}) \quad (6)$$
$$Q_{22} = E_2/(1 - \nu_{12}\nu_{21})$$
$$Q_{66} = G_{12}$$

2.3 Database of double angle-ply laminate configurations with non-crimp fabrics (NCF).

Double angle-ply non-crimp fabric architectures are now available commercially and with bespoke ply angles. Hence the new database presented in this article contains stacking sequence listings in symbolic form together with non-dimensional parameters, to which any fibre angle, ply thickness and material properties can be later assigned, and the stiffness properties readily determined, as above.

Solutions are derived algorithmically, using a similar procedure to that for Standard angle designs [12], but the range of ply number groupings is now extended to n = 24. Individual layers are now represented by four possible combinations of balanced angle-ply pairings: $\underline{\psi/-\psi}$, $\underline{-\psi/\psi}$, $\underline{\phi/-\phi}$ and $\underline{-\phi/\phi}$. In general, it is assumed that $\phi \neq \psi$ and $-90° \leq (\phi, \psi) \leq 90°$. The number of possible solutions is therefore $4^{(n/2-1)}$ since the first layer, $\underline{\psi/-\psi}$, is assumed to be fixed. This is also consistent with design rules for laminate thickness tapering, involving ply terminations, where the outer ply should generally be continuous throughout the structure or component. The ply contiguity constraint, or so-called ply blocking rule, can be dismissed completely when adopting double angle-ply non-crimp fabric designs, since ply contiguity is now limited to a maximum of 2 adjacent plies with identical orientation.

The number of solutions is reported in Table 6 as Uncoupled NCF. These results suggest that there are very few practical designs possessing fully uncoupled properties. A modified algorithm was employed to assess the number of *Bending-Twisting* coupled NCF designs, for which D_{16}, $D_{26} \neq 0$. These are also presented in Table 6, for the comparison purposes, but are not discussed further in this article.

Lamination parameters [26] offer an more appropriate set of non-dimensional expressions when ply angles are a design variable, as is the case for double angle-ply configurations. The resulting lamination parameters can also be presented graphically to help with the design process. Lamination parameters are also pertinent to the stiffness matching procedure described in the following section.

The relationship between the non-dimensional parameters developed in the previous section and the angle ply dependent lamination parameters relating to extensional and bending stiffness, are given by [13]:

$$\begin{aligned} \xi_1 &= \{n_{\pm\psi}\cos(2\psi) + n_{\pm\phi}\cos(2\phi)\}/n & \xi_9 &= \{\zeta_{\pm\psi}\cos(2\psi) + \zeta_{\pm\phi}\cos(2\phi)\}/\zeta \\ \xi_2 &= \{n_{\pm\psi}\cos(4\psi) + n_{\pm\phi}\cos(4\phi)\}/n & \xi_{10} &= \{\zeta_{\pm\psi}\cos(4\psi) + \zeta_{\pm\phi}\cos(4\phi)\}/\zeta \end{aligned} \tag{7}$$

Stacking sequences and their corresponding non-dimensional parameters, $n_{\pm\psi}$, $n_{\pm\phi}$, $\zeta_{\pm\psi}$ and $\zeta_{\pm\phi}$, are provided in Tables 7 and 8 for NCF designs. The complete list of designs, together with graphical representations of the lamination parameter design spaces, corresponding to extensional and bending stiffness, are given in Appendix 3: Double Angle-Ply Designs Derived from Standard-Ply Designs, for UD designs. The extensional and bending stiffness matrices, for laminate thickness H (= $n \times t$), are readily calculated from the lamination parameter coordinates, using the following equations:

$$\begin{aligned} A_{11} &= \{U_1 + \xi_1 U_2 + \xi_2 U_3\} \times H & D_{11} &= \{U_1 + \xi_9 U_2 + \xi_{10} U_3\} \times H^3/12 \\ A_{12} = A_{21} &= \{-\xi_2 U_3 + U_4\} \times H & D_{12} = D_{21} &= \{-\xi_{10} U_3 + U_4\} \times H^3/12 \\ A_{22} &= \{U_1 - \xi_1 U_2 + \xi_2 U_3\} \times H & D_{22} &= \{U_1 - \xi_9 U_2 + \xi_{10} U_3\} \times H^3/12 \\ A_{66} &= \{-\xi_2 U_3 + U_5\} \times H & D_{66} &= \{-\xi_{10} U_3 + U_5\} \times H^3/12 \end{aligned} \quad (8)$$

where laminate invariants, U_i, are calculated from the reduced stiffness terms, Q_{ij}:

$$\begin{aligned} U_1 &= \{3Q_{11} + 3Q_{22} + 2Q_{12} + 4Q_{66}\}/8 & U_2 &= \{Q_{11} - Q_{22}\}/2 \\ U_3 &= \{Q_{11} + Q_{22} - 2Q_{12} - 4Q_{66}\}/8 & U_4 &= \{Q_{11} + Q_{22} + 6Q_{12} - 4Q_{66}\}/8 \\ & & U_5 &= \{Q_{11} + Q_{22} - 2Q_{12} + 4Q_{66}\}/8 \end{aligned} \quad (9)$$

2.4 Stiffness matching algorithm

Lamination parameters can be matched precisely to the stiffness requirements by employing numerical optimisation routines, but matching the lamination parameters to stacking sequence that can be manufactured, and more importantly tapered or blended to adjacent structure, is an ongoing research topic. A tailoring strategy is therefore developed here to achieve specific characteristics in either bending or extensional stiffness for the databases of double angle-ply designs, consisting of either non-crimp fabrics, or UD layers. The algorithm matches the bending stiffness of double angle-

ply laminates, with $\pm\phi$ and $\pm\psi$ fibre directions to that of standard-ply laminates (with 0°, ±45° and 90° fibre directions) or indeed any target design defined by its lamination parameters.

The standard-ply angle configurations containing 0°, 90° and ±45° plies, for spar, skin and stiffener are now replaced by double angle ply $[\pm\phi_{(\gamma)}/\pm\psi_{(1\ -\ \gamma)}]$ laminates, where subscript γ represents the proportion of the $\pm\phi$ sub-laminate, and remainder $(1 - \gamma)$ represents the proportion of $\pm\psi$ sub-laminate. For extension stiffness matching, these proportions simply correspond to the ply percentages of $\pm\phi$ and $\pm\psi$ plies in the laminate.

As an example, designing with double angle-ply laminates can facilitate the use of a fixed angle ($\pm\phi = \pm60°$) sub-laminate, together with a component dependent variable angle sub-laminate ($\pm\psi$). These angle combinations are illustrated on the parabola, defining the feasible region of lamination parameters on the design space of Fig. 2, with coordinates derived from Eqn (7). Broken lines, joining two of these specific double angle-ply coordinates, pass through the respective lamination parameter coordinates of each component. For a fixed angle ($\pm\phi = \pm60°$), the hypothetical proportions of each of the two double angle plies are derived from a standard lever rule calculation and correspond to the ply percentages given in parentheses: Spar $[\pm60_{(44.4\%)}/\pm33.2_{(55.6\%)}]$, Skin $[\pm60_{(40.5\%)}/\pm14.3_{(59.5\%)}]$, and Stiffener $[\pm60_{(31\%)}/\pm9.1_{(69\%)}]$.

Ply percentages are generally insufficient for practical design purposes, even when they are applied only to extensional stiffness. The usual design procedure is to develop a series of symmetric solutions, since these guarantee that thermal warping is eliminated, i.e., flat plates remain flat after high temperature curing. However, symmetric designs do not guarantee that *Bending-Twisting* coupling is eliminated and it is has been previously demonstrated that only a very small percentage of symmetric laminates are fully uncoupled [14]. Stacking sequence configurations are therefore chosen from the databases developed in the previous section, from which there are in fact no symmetric double angle-ply designs.

The tailoring strategy focuses on matching lamination parameter coordinates for bending stiffness (ξ_9, ξ_{10}), or extensional stiffness (ξ_1, ξ_2), to achieve improvements structural performance using double

angle-ply laminates in place of their standard-ply counterparts.

The ply angle dependent lamination parameters (ξ_9, ξ_{10}) are related to non-dimensional parameters, derived earlier, which represent the summation of the relative contribution to bending stiffness of the fixed ply angles of the standard laminate, where symbols ○, +, – and ● are assumed to represent standard angles 0, +45, -45 and 90°:

$$\begin{aligned}\xi_9 &= \{\zeta_{○}\cos2\theta_{○} + \zeta_{+}\cos2\theta_{+} + \zeta_{-}\cos2\theta_{-} + \zeta_{●}\cos2\theta_{●}\}/\zeta \\ \xi_{10} &= \{\zeta_{○}\cos4\theta_{○} + \zeta_{+}\cos4\theta_{+} + \zeta_{-}\cos4\theta_{-} + \zeta_{●}\cos4\theta_{●}\}/\zeta\end{aligned} \tag{10}$$

For balanced angle ply contributions, ζ_+ and ζ_-, may be combined:

$$\begin{aligned}\xi_9 &= \{\zeta_{○}\cos2\theta_{○} + \zeta_{(+/-)}\cos2\theta_{(+/-)} + \zeta_{●}\cos2\theta_{●}\}/\zeta \\ \xi_{10} &= \{\zeta_{○}\cos4\theta_{○} + \zeta_{(+/-)}\cos4\theta_{(+/-)} + \zeta_{●}\cos4\theta_{●}\}/\zeta\end{aligned} \tag{11}$$

Replacing the equal contributions from orthotropic plies ○ and ● with variable angle-ply pairs $(+\phi/-\phi)$ and $(-\phi/+\phi)$, respectively, and fixed standard angle plies + and – with variable angle-ply pairs $(+\psi/-\psi)$ and $(-\psi/+\psi)$, gives:

$$\begin{aligned}\xi_9 &= \{\zeta_{(+\phi/-\phi)}\cos2\theta_{(+\phi/-\phi)} + \zeta_{(-\phi/+\phi)}\cos2\theta_{(-\phi/+\phi)} + \zeta_{(+\psi/-\psi)}\cos2\theta_{(+\psi/-\psi)} + \zeta_{(-\psi/+\psi)}\cos2\theta_{(-\psi/+\psi)}\}/\zeta \\ \xi_{10} &= \{\zeta_{(+\phi/-\phi)}\cos4\theta_{(+\phi/-\phi)} + \zeta_{(-\phi/+\phi)}\cos4\theta_{(-\phi/+\phi)} + \zeta_{(+\psi/-\psi)}\cos4\theta_{(+\psi/-\psi)} + \zeta_{(-\psi/+\psi)}\cos4\theta_{(-\psi/+\psi)}\}/\zeta\end{aligned} \tag{12}$$

Once again, for balanced angle-ply pairings, contributions, $\zeta_{(+\psi/-\psi)}$ and $\zeta_{(-\psi/+\psi)}$, as well as $\zeta_{(+\phi/-\phi)}$ and $\zeta_{(-\phi/+\phi)}$, may be combined and expressed as:

$$\xi_9 = \{(\zeta_{\pm\phi})\cos2\phi + (\zeta_{\pm\psi})\cos2\psi\}/\zeta \qquad \xi_{10} = \{(\zeta_{\pm\phi})\cos4\phi + (\zeta_{\pm\psi})\cos4\psi\}/\zeta \tag{13}$$

and given $\zeta = \zeta_{\pm\phi} + \zeta_{\pm\psi}$ (= n^3), where ζ is a non-dimensional parameter corresponding to the total contribution to bending stiffness for all *n* plies in the laminate, the expression becomes:

$$\xi_9 = \{(\zeta_{\pm\phi})\cos2\phi + (\zeta - \zeta_{\pm\phi})\cos2\psi\}/\zeta \qquad \xi_{10} = \{(\zeta_{\pm\phi})\cos4\phi + (\zeta - \zeta_{\pm\phi})\cos4\psi\}/\zeta \qquad (14)$$

or can be simplified further using $\gamma = \zeta_{\pm\phi}/\zeta$, and $\alpha = \cos2\phi$ and $\beta = \cos2\psi$, and the double angle relationship $\{\cos4\phi = 2\cos^2(2\phi) - 1\}$ to give:

$$\xi_9 = (\zeta_{\pm\phi}/\zeta)\alpha + (1 - \zeta_{\pm\phi}/\zeta)\beta \qquad \xi_{10} = (\zeta_{\pm\phi}/\zeta)(2\alpha^2 - 1) + (1 - \zeta_{\pm\phi}/\zeta)(2\beta^2 - 1) \qquad (15)$$

From the first of the expressions in Eqn. (15) the relative contributions to bending stiffness of the $\pm\phi$ sub-laminate becomes:

$$\zeta_{\pm\phi}/\zeta = (\xi_9 - \beta)/(\alpha - \beta) \qquad (16)$$

where $\zeta_{\pm\phi}/\zeta$ is established from the database.

Finally, substituting Eqn. (16) into the second expression of Eqn (15) leads to the following quadratic solution for β (= $\cos2\psi$):

$$\beta = -(\xi_{10} + 1 - 2\alpha^2)/4(\alpha - \xi_9) \pm [((\xi_{10} + 1 - 2\alpha^2)/4(\alpha - \xi_9))^2 - (2\alpha^2\xi_9 - \alpha - \xi_{10}\alpha)/2(\alpha - \xi_9)]^{1/2} \qquad (17)$$

The value of α (= $\cos2\phi$) is solved iteratively until Eqn. (16) is balanced, using the target value of β (= $\cos2\psi$) from Eqn. (17), which contains the lamination parameter coordinates (ξ_9, ξ_{10}) of interest. The angle ψ is then solved directly through $\beta = \cos2\psi$, once the iterative process has converged.

Note that this strategy can also be applied to matching of lamination parameter coordinates (ξ_1, ξ_2) for extensional stiffness using any designs from the databases given in Appendix 2 - Double Angle-

Ply Designs Derived from Standard-Ply Designs and using Eqs (7), or Appendix 3 - Double Angle-Ply Designs.

To demonstrate the tailoring strategy, designs with bending isotropy have been listed in Table 7 for the 16 ply solutions. Bending stiffness proportions ($\zeta_{\pm\phi}/\zeta$) and ($\zeta_{\pm\psi}/\zeta$) are given together with angles (ϕ_{Iso}, ψ_{Iso}) for designs that lead to bending isotropy. Ply proportions ($n_{\pm\phi}/n$) = ($n_{\pm\psi}/n$) = 0.5 for all designs and give therefore lead to extensional isotropy for (ϕ_{Iso}, ψ_{Iso}) = (67.5°, 22.5°).

Table 8 also lists example stacking sequences corresponding to the 15 groups of fully uncoupled double angle-ply laminate with 24 layers. These are split into Tables 8(a) with ply proportions ($n_{\pm\phi}/n$, $n_{\pm\psi}/n$) = (0.67, 0.33) and Tables 8(b) with ($n_{\pm\phi}/n$, $n_{\pm\psi}/n$) = (0.33, 0.67). Bending stiffness proportions ($\zeta_{\pm\phi}/\zeta$) and ($\zeta_{\pm\psi}/\zeta$) are given together with angles (ϕ_{Iso}, ψ_{Iso}) for designs that lead to bending isotropy.

Note that the database of double angle-ply laminates with 24 layers contains 108 designs, which are split into 15 groups of between 6 and 8 designs with identical extensional and bending stiffness characteristics.

2.5 Lamination parameter design space representation

New lamination parameter design space representations are now developed for variable double angle-ply laminates, to help with the design process. These design space representations differ considerably from those of standard-ply designs. First of all, the designs now fall within parabolic bounds, represented by $\xi_{10} = 2\xi_9^2 - 1$, rather than the triangular bounds of standard ply angles 0°, ±45° and 90°, illustrated in Fig. 2. Secondly, two infeasible regions now exist within these parabolic bounds, which are themselves parabolic in nature, and depend on the specific sub-laminate proportions, i.e. ply percentages.

Figure 3(a) represents the lamination parameter design space in extensional stiffness (ξ_1, ξ_2) for all fully uncoupled double angle-ply laminates with 16 plies, which are listed in Table 7. Isolines, representing constant ply angles $\pm\phi$ with variation in $\pm\psi$, or vice versa, have been superimposed on the design spaces, to help interrogation of the lamination parameter coordinates for any angle-ply

combination; 10° intervals are used to aid interpolation.

Two specific angle-ply combinations are highlighted on Fig. 3(a). The first has $(\pm\phi, \pm\psi) = (\pm\phi_{Iso}, \pm\psi_{Iso}) = (\pm 74.45°, \pm 27.14°)$, and is represented by two corresponding points on the parabolic bounds of the design space, between which a broken line provides a Lever rule representation passing through the lamination parameter coordinate for extensional stiffness. The coordinate, $(\xi_1, \xi_2) = (-0.14, 0.07)$, is determined by the relative proportion of each angle-ply sub-laminate. All 16-ply laminates share the ply proportions $(n_{\pm\phi}/n) = (n_{\pm\psi}/n) = 0.5$, i.e., Fig. 3 represents the design space for all stacking sequences listed in Table 7. Extensional isotropy exists when the lamination parameter coordinate $(\xi_1, \xi_2) = (0, 0)$, as illustrated by the second angle-ply combination, which corresponds to $(\phi_{Iso}, \psi_{Iso}) = (67.5°, 22.5°)$.

Figure 3(c) illustrates the coordinate for the first angle-ply combination, with $(\pm\phi_{Iso}, \pm\psi_{Iso}) = (\pm 74.45°, \pm 27.14°)$, which can be seen to give rise to Isotropy in bending, i.e., $(\xi_9, \xi_{10}) = (0, 0)$. The broken line Lever rule representation depends now on the relative proportion that each angle-ply sub-laminate contributes to the overall bending stiffness, $(\zeta_{\pm\phi}/\zeta)$ and $(\zeta_{\pm\psi}/\zeta)$, which differs between the designs in Table 7. The second angle-ply combination, representing $(\pm\phi, \pm\psi) = (67.5°, 22.5°)$, corresponds to the lamination parameter coordinate $(\xi_9, \xi_{10}) = (0.13, 0.00)$.

Note that if the angle ply pairs are switched, ϕ with ψ and vice versa, giving $[\underline{\phi/-\phi}/\underline{\psi/-\psi}/\underline{-\psi/\psi}/\underline{-\phi/\phi}]_A$, the first angle-ply combination becomes $(\pm\phi_{Iso}, \pm\psi_{Iso}) = (\pm 62.95°, \pm 15.74°)$. The switched angles simply correspond to $(90-\psi, 90-\phi)$. The second angle-ply combination becomes $(\pm\phi, \pm\psi) = (22.5°, 67.5°)$. Switching the angles in the way results in a mirror image of the entire set of design spaces shown in Figs 3.

Figure 3(b) illustrates the lamination parameter design space in bending (ξ_9, ξ_{10}) for laminates *a* and *b* of Table 7, which are also stiffness matched. Similarly, Fig. 3(d) illustrates the bending stiffness design space for laminates *e* and *f* of Table 7. However, both reveal large infeasible regions within the parabolic bounds that preclude the possibility of achieving bending isotropy, $(\xi_9, \xi_{10}) = (0.00, 0.00)$, for any ply angle combinations. These design do however offer an advantage over the designs shown

in Fig. 3(c), given that their lamination parameters are relatively insensitive to changes in one of ply angle pairs, which has potential for improvements in buckling strength performance.

A further 15 graphical representations, or design charts, for extensional and bending stiffness are provided in Appendix 3 - Double Angle-Ply Designs, which cover the entire database of 24 ply designs. They highlight bending isotropy in designs for which this is possible in bending and/or extension. Lamination parameter (ξ_1, ξ_2) for typical spar, skin and stiffener components are also highlighted, together with the corresponding (ξ_9, ξ_{10}) locations within the design space.

2.6 Laminate Tapering through Ply Terminations

A number of studies have revealed the extent to which taper is possible in standard laminates, balanced plain weave and non-crimp fabric (NCF) laminate designs with single-ply or, where necessary, multiple-ply terminations, to investigate the extent to which individual layers can be terminated without introducing undesirable mechanical coupling, or warping distortions [17 - 19].

Tapered laminate designs have been developed in a top down process, in which each ply number grouping, comprising n layers, is filtered through a lower ply number grouping $n - m$, resulting from m layer terminations. However, Table 6 reveals that Uncoupled NCF exist only for 16 and 24 ply number groupings, hence $n = 24$ and $m = 8$, noting that 8 UD plies equate to 4 NCF layers.

The termination scheme involves m ply terminations, applied to all combinations in every stacking sequence with n ply layers; comparison with all stacking sequences with $n - m$ plies and; recording exact matches. The first (or upper surface) ply is assumed to be continuous throughout the tapering process; this represents a practical design constraint to prevent surface ply delamination. This constraint would also be applied to the last (or lower surface) ply in design practice, however, the results have been reported here to reveal the propensity for such terminations. In fact, surface ply terminations may offer the possibility for ply continuity into an outstand component, such as a stiffener. Some examples are highlighted here only for solutions with good dispersal of terminated NCF layers, since some tapered solutions do involve the termination of ply blocks with 2 or more

adjacent NCF layers. All of the 16 ply designs from Table 7 are found to have one or more compatible 24 ply designs. For example Laminate 16*a* is compatible with either Laminates 24*n*(1) or 24*o*(1):

24*n*(1): [ψ/−ψ/**ψ/−ψ**/−ψ/ψ/**−ϕ/ϕ**/−ψ/ψ/ϕ/−ϕ/ϕ/−ϕ/−ψ/ψ/**−ϕ/ϕ**/−ψ/ψ/ψ/−ψ/**ψ/−ψ**]$_T$

16*a*: ψ/−ψ/−ψ/ψ/−ϕ/ϕ/ϕ/−ϕ/ϕ/−ϕ/−ϕ/ϕ/−ψ/ψ/ψ/−ψ]$_T$

24*o*(1): [ψ/−ψ/**ψ/−ψ**/−ψ/ψ/**−ψ/ψ**/−ϕ/ϕ/ϕ/−ϕ/ϕ/−ϕ/−ϕ/ϕ/−ψ/ψ/**−ψ/ψ**/ψ/−ψ/**ψ/−ψ**]$_T$

Similar termination patterns are seen in the other 16 ply designs: 16*b* is compatible with 24*n*(2) or 24*o*(2), 16*c* with 24*j*(1) or 24*k*(1), 16*d* with 24*l*(1), 16*e* with 24*l*(6), and 16*f* with 24*j*(6) or 24*k*(6).

Certain designs have been discarded from the database for the purposes of practical tapering but are reported here because they offer an alternative to the use of metallic tabs for experimental purposes, to avoid local effects from the mechanical grips, using top and bottom surface ply bocks **ψ/−ψ/−ψ/ψ** and **−ψ/ψ/ψ/−ψ**, respectively. They form a common design configurations applicable to all 16-ply designs from Table 7, and do not introduce mechanical coupling. Laminate 24*o*(3) represents the tabbed layup for Laminate16*a*:

24*o*(3): [**ψ/−ψ/−ψ/ψ**/ψ/−ψ/−ψ/ψ/−ϕ/ϕ/ϕ/−ϕ/ϕ/−ϕ/−ϕ/ϕ/−ψ/ψ/ψ/−ψ/**−ψ/ψ/ψ/−ψ**]$_T$

16a*:* [ψ/−ψ/−ψ/ψ/−ϕ/ϕ/ϕ/−ϕ/ϕ/−ϕ/−ϕ/ϕ/−ψ/ψ/ψ/−ψ]$_T$

This can be written as [**ψ/−ψ/−ψ/ψ**/ 16*a* /**−ψ/ψ/ψ/−ψ**]$_T$

Applying these surface ply blocks to laminates 16*b* – 16*f*, gives rise, respectively, to laminates 24*o*(4), 24*m*(4), 24*n*(4), 24*n*(3), and 24*m*(3), from Appendix 3 - Double Angle-Ply Designs.

The following stacking sequences were not compatible with any of the 16 ply designs from Table 7: Laminates 24*e*(2) – (3), 24*h*(3), 24*i*(3), 24*l*(7), and 24*n*(6).

3 BUCKLING SIMULATION RESULTS AND DISCUSSION

This section presents a selection of buckling design charts applicable to both double angle-ply and standard-ply designs, which can be used to gain insights into gaining a specific buckling performance threshold through appropriate choice of ply angles. The effect of tailored double angle-ply designs with matched isotropic properties in bending are also used to demonstrate the influence of variation in axial stiffness on the stability of a classical thin walled z-sections column with simply supported and clamped ends.

Analyses were performed with the VICONOPT computer code [20], which is based on the stiffness-matrix method with exact flat plate theory. Two types of analysis are used, which are based on those of the earlier programs VIPASA and VICON. The theory of VIPASA (vibration and instability of plate assemblies with shear and anisotropy) analysis assumes that the mode of buckling varies sinusoidally in the longitudinal direction with half wavelength λ. Nodal lines, or lines of zero buckling displacement, are straight and perpendicular to the longitudinal direction, that is, in the transverse direction, if all plates are orthotropic and no shear loading is present. Simply supported end conditions are satisfied in this case. Otherwise, solutions only approximate such end conditions and become excessively conservative as λ approaches the panel length. VICON (VIPASA with constraints) theory uses Lagrangian multipliers to impose the constraints representing point supports, so that, for instance, a shear loaded panel supported along rectangular boundaries can be accurately represented. To achieve this, the analysis combines stiffness matrices for different wavelengths, derived from the VIPASA theory, to enforce the required number and location of nodal points in the resulting mode shape. Thus, results are for an infinitely long plate assembly, with supports repeating at panel length intervals, see Fig. 4. The VIPASA theory is sufficient for the infinitely long plate assumption, used to generate the buckling results that follow, hence the results can be verified using the PASCO computer code [21]. The optimisation features in these codes allow for design variables such as ply angles along with geometric parameters and material strength constraints [22-24], however these features are not employed for the results that follow. Instead, the design of stiffness properties is achieved through the tailoring method presented earlier.

3.1 Infinitely long plates in compression or shear loading

Infinitely long plate assumption, with simple supports represent idealized boundary conditions compared to those of the real structure but do represent lower bound buckling solutions and are therefore the most useful in preliminary design. The relationship between simple supports and other boundary conditions is now well understood and is covered extensively in the literature [25], albeit predominantly for metallic (isotropic) plates. The results presented here therefore adopt an equivalent isotropic laminate datum to bridge the gap between metallic and composite behaviour. Buckling results for composite plates with finite length can also be found elsewhere [16].

There are many published results dealing with the design of laminated composite plate assemblies or build up structure subject to buckling constraints. However, buckling behaviour cannot be generalized in such cases, because it is usually configuration dependent [22-24]. By contrast, results from the current study are applicable where plate assemblies exhibit local buckling of the individual plates between or within stiffeners and spars. The focus here is therefore to provide insight into the possibilities for laminate stiffness tailoring of double angle-ply designs which are immune to the degrading effects of bending-twisting coupling, particularly in compression loaded plates, or to exploit the beneficial effects where plates are shear loaded.

Compression and shear buckling contours are mapped onto the lamination parameter design space of Fig. 5 so that they can be compared side by side with the double angle-ply design charts of Fig. 3 for 16 ply designs and the 24 ply designs of Appendix 3 - Double Angle-Ply Designs. The isolines represent non-dimensional compression and shear buckling factors, $k_{x,\infty}$ (= $N_{x,\infty}b^2/\pi^2 D_{Iso}$) and $k_{xy,\infty}$ (= $N_{xy,\infty}b^2/\pi^2 D_{Iso}$), for infinitely long plates with simply supported edges. D_{Iso} corresponds to D_{11} of Eq. (8) with (ξ_9, ξ_{10}) = (0, 0), representing the bending stiffness of the equivalent Isotropic laminate. This normalisation ensures that buckling factor results are comparable across the design space, since the relative change in buckling factor, k_x or k_{xy}, is the same as the relative change in the critical force resultant, N_x or N_{xy}.

Figure 5(a) identifies skin panel designs of Table 3, whereas Fig. 5(b) identifies spar designs of Table 4. The feasible region of lamination parameters for standard-ply designs is indicated by broken lines. Individual isolines are developed from the following lamination parameter expressions [14,15]:

$$k_{x,\infty} = 4.000 - 1.049\xi_{10} - 1.217\xi_9^{\,2} + 0.34\xi_9^{\,2}\xi_{10} - 0.360\xi_9^{\,4} - 0.034\xi_9^{\,2}\xi_{10}^{\,2}$$

$$\begin{aligned} k_{xy,\infty} = {} & 5.336 - 2.914\xi_9 - 0.518\xi_{10} - 1.303\xi_9^{\,2} - 0.213\xi_{10}^{\,2} + 1.048\xi_9\xi_{10} - 0.236\xi_9^{\,3} + 0.031\xi_{10}^{\,3} - 0.197\xi_9\xi_{10}^{\,2} \\ & + 0.405\xi_9^{\,2}\xi_{10} - 0.443\xi_9^{\,4} - 0.001\xi_{10}^{\,4} + 0.022\xi_9\xi_{10}^{\,3} - 0.185\xi_9^{\,2}\xi_{10}^{\,2} + 0.472\xi_9^{\,3}\xi_{10} \end{aligned} \qquad (18)$$

The lamination parameters (ξ_9, ξ_{10}) can be found for all standard and double angle-ply laminates, either directly or graphically within Appendices 1 – 3.

These expressions were developed using exact buckling factor results from VICONOPT, at 15 equally spaced grid points across the lamination parameter design space and correspond specifically to Graphite/Epoxy IM7/8552. These expressions were also used to generate the buckling factor results associated with the laminate designs of Tables 2 - 4. Note that for other materials, the buckling factors are equal only for the equivalent isotropic material properties, i.e. (ξ_9, ξ_{10}) = (0, 0) on Fig. 5, and correspond to the classical buckling factor results, $k_{x,\infty} = 4.0$ and $k_{xy,\infty} = 5.336$ for metallic plates [25]. There is a relative magnification in buckling factor as a result of the different material orthotropies in the fibre/matrix properties listed in Table 1, hence each material has a unique set of coefficients. Scotchply 1002 Glass/Epoxy has, for instance, the following lamination parameter expressions:

$$k_{x,\infty} = 4.000 - 0.651\xi_{10} - 0.57\xi_9^{\,2} + 0.09\xi_9^{\,2}\xi_{10} - 0.07\xi_9^{\,4} - 0.002\xi_9^{\,2}\xi_{10}^{\,2}$$

$$\begin{aligned} k_{xy,\infty} = {} & 5.336 - 2.009\xi_9 - 0.318\xi_{10} - 0.62\xi_9^{\,2} - 0.082\xi_{10}^{\,2} + 0.449\xi_9\xi_{10} - 0.054\xi_9^{\,3} + 0.006\xi_{10}^{\,3} - 0.04\xi_9\xi_{10}^{\,2} \\ & + 0.089\xi_9^{\,2}\xi_{10} - 0.075\xi_9^{\,4} - 0.02\xi_9^{\,2}\xi_{10}^{\,2} + 0.068\xi_9^{\,3}\xi_{10} \end{aligned} \qquad (19)$$

The general shape of the buckling contours are similar to those in Fig. 5 but the magnitude of the buckling factor changes towards the boundaries of the lamination parameter design space. For laminates with 0° or 90° plies only, the relative compression buckling factor, $k_{x,\infty}$, of Glass/Epoxy is

66% higher than Graphite/Epoxy, whilst for laminate containing only ±45° plies, $k_{x,\infty}$ is 8% lower. The shear buckling factor, $k_{xy,\infty}$, is 109% or 20% higher for laminates with 0° or 90° plies only, and 1% lower for laminates containing only ±45° plies.

The shear buckling contours of Fig. 5(b) suggest Laminate *a* and *b* of Table 7 can achieve the highest shear buckling performance threshold, corresponding to $k_{xy,\infty} = 6.93$, for any angle ϕ when paired with $= \psi 60°$, as seen from the design space shown in Fig. 3(b).

Bounds on the buckling performance of infinitely long, simply supported, symmetric laminates have been thoroughly investigated previously using approximate closed form buckling solutions [27]. For the infinitely long compression loaded plate with simply supported edges, the closed form solution is given by:

$$k_{x,\infty} = N_{x,\infty} b^2/\pi^2(D_{11}D_{22})^{½} = 2(1 + \beta) \tag{20}$$

where:

$$\beta = (D_{12} + 2D_{66})/(D_{11}D_{22})^{1/2} \tag{21}$$

In view of the significant number of non-symmetric and other forms of sub-sequence symmetry identified elsewhere [12], representing a design space containing 46,682 solutions, after applying the 10% rule and continuity constraints adopted throughout this article, the additional gains in buckling performance above symmetric laminates are revealed in Table 2. However, for these normalized results, $k_{x,\infty}$ is disproportional to the buckling results, $N_{x,\infty}$, due to the use of $(D_{11}D_{22})^{½}$ rather than D_{Iso}. For comparison between the two different normalisation procedures, Eqn (20) must be factored by $(D_{11}D_{22})^{½}/D_{Iso}$. Comparison with first of Eqns (18) reveals a 0.0% difference, which is unsurprising given that these results can also be readily verified using the exact closed form solution (with half-wavelength λ):

$$N_{x,\infty} = \pi^2 \left[D_{11} \left[\frac{1}{\lambda} \right]^2 + 2(D_{12} + 2D_{66}) \frac{1}{b^2} + D_{22} \left[\frac{1}{b^4} \right] \lambda^2 \right] \quad (22)$$

For the infinitely long shear loaded plate with simply supported edges, the closed form solution is given by:

$$k_{xy,\infty} = N_{xy,\infty} b^2/\pi^2 (D_{11} D_{22}^3)^{1/4} = 3.32 + 2.16 - \beta 0.16\beta^2 \quad (23)$$

Note that the shear buckling equation is normalized differently from the equation for compression buckling and is again disproportional to the shear buckling results, $N_{xy,\infty}$. Factoring Eqn (23) by $(D_{11}D_{22}^3)^{1/4}/D_{Iso}$, reveals differences of between -0.4% and 0.2% from the equations presented herein, applied to the entire orthotropic laminate database, irrespective of the form of subsequence symmetry.

3.2 Thin walled column buckling under compression loading

The consideration of stability loss through local, global and interactive forms of buckling and in particular the effective length at which such forms transition, remains a subject of much interest [28], particularly in the context of composite materials and the added complexities that are involved [29].

In this section the classical problem of a Z-section column in compression is presented to highlight the benefits of adopting double angle-ply designs with matching isotropic properties in bending, but with differing extensional stiffness characteristics. VICONOPT is used for computation expedience, since the theory assumes as a series of infinite strips, rather than finite elements, hence only the cross-sectional geometry need be defined; boundaries conditions are enforced at repeating intervals, corresponding to the desired column length. For compression buckling problems, the mode shapes are either equal and/or opposite in adjacent bays and therefore give identical buckling loads to the finite length column results from a finite element analysis, but without requiring a mesh refinement for each of the column lengths investigated. Clamped ends imply that the infinitely long representation degenerates into finite length column between clamped supports.

Figure 6 presents a comparison of the compression buckling curves for a Z-section column, with 40mm flanges and an 80mm web, for both simply supported and clamped ends. The material properties used correspond to AS/3501 Graphite/Epoxy of Table 1, since these match closely the properties of the North Thin Ply Technology unidirectional pre-preg material TP513/34-700/75gsm/36% used to manufacture the 24-ply test specimens. The sections were manufactured in a closed aluminum mold with an internal radius at the flange/web intersection of 2mm, which were not modelled. The measured wall thickness was 1.6mm. There was no visible distortion in the specimen and the test data was found to produce good correlation to the local buckling predictions, using back to back strain gauges at mid length.

The buckling curves Fig. 6 represent double angle-ply designs from Table 8 for which more detailed experiments are planned, with bending stiffness matched to the fully isotropic datum configuration with 24 plies, $[45/90/0/-45/0/-45/90/-45/45/0/45/90/45/90/-45/90/0/45/0/-45/0/-45/45/90]_T$. Matched Isotropy in bending stiffness is obtained using the $\{\phi\pm/\psi\pm\}$ combinations shown. Note that the double angle-ply design, labelled Laminate *d*, is also used with angles switched from $\{\pm27.1\pm/74.3\}$ to $\{\pm62.9\ \pm/15.7\}$, thus modifying the axial stiffness without affecting the bending isotropy. These results demonstrate that laminate tailoring of double angle-ply laminates in bending can lead to increases in the effective length and that the onset of overall buckling can be delayed through appropriate choice of axial stiffness, without affecting the local buckling load carrying capacity of the column.

4 CONCLUSIONS

This article has demonstrated the benefits of double angle-ply designs compared to standard-ply designs with balanced and symmetric stacking sequences.

Symmetric designs have been shown to severely limit the scope for design of typical aircraft components, such as spars, skins or stiffeners, particularly in thin laminates if *Bending-Twisting* coupling is to be eliminated, along with the associated detrimental effects that this has on buckling performance. Furthermore, the buckling performance of symmetric designs has been shown never to

exceed that of the equivalent non-symmetric design.

Double angle-ply designs are also limited, both in terms of the number of available configurations and ply number groupings, especially when non-crimp fabric architectures are employed. However, such designs benefit from the fact that they can be tailored in either extensional or bending stiffness, by a suitable choice of ply orientations, covering most of the feasible design space.

Stiffness tailoring has been demonstrated through a stiffness matching algorithm and new design charts provide the specific angle combinations to achieve desirable lamination parameter coordinates.

Designing for precisely matched stiffness in bending leads to identical local buckling strength in plates. Such designs are readily determined from the lamination parameter design charts onto which isolines of constant buckling factor have been mapped. These charts account for infinitely long plates with simply supported edges in either compression or shear.

Bending stiffness matching has also allowed the effect of axial stiffness to be realised for thin walled compression members. This has been shown to increase the effective length of the member by delaying the transition from local to overall buckling.

The stiffness matching approach is underpinned by design data presented in a comprehensive set of appendices, including a full listing of tapered designs for blended structures. These have potential benefit for blending between compression and shear dominant regions by maintaining one angle throughout and modifying the second angle on each side of the zone around which plies are terminated.

Data Sets:

The following electronic appendices can be accessed at: York, Christopher (2020), "Laminate Stiffness Tailoring for Improved Buckling Performance", Mendeley Data, V1, doi: 10.17632/v2h5h5vdcc.1

Appendix 1 - Balanced and Symmetric Standard-Ply Designs

Appendix 2 - Double Angle-Ply Designs Derived from Standard-Ply Designs

Appendix 3 - Double Angle-Ply Designs

Appendix 4 - Tapered Double Angle-Ply Designs

Acknowledgements

Aspects of this research were supported by the Engineering and Physical Sciences Research Council grant EP/S013555/1 and Ministry of Education grants R-MOE-E103-D020 and R-MOE-A403-G011.

REFERENCES

[1] S.W. Tsai. Weight and cost reduction by using unbalanced and unsymmetric laminates. Proc. 18th International Conference on Composite Materials, Jeju, Korea (2011)

[2] M. Papila. Design of and with thin-ply non-crimp fabric as building blocks for composites. Science and Engineering of Composite Materials, 25(3) (2018) 501–516.

[3] S.W. Tsai. Design of composite laminates, 21st International Conference on Composite Materials, Xi'an, China (2017)

[4] S.W. Tsai, J.D.D. Melo, S. Sihn, A. Arteiro, R. Rainsberger. Composite Laminates: Theory and practice of analysis, design and automated layup. Composites Design Group, Stanford University (2017)

[5] M.W.D. Nielsen, K.J. Johnson, A.T. Rhead, R. Butler. Laminate design with non-standard ply angles for optimised in-plane performance, 21st International Conference on Composite Materials, Xi'an, China (2017)

[6] M.W.D. Nielsen, K.J. Johnson, A.T. Rhead, R. Butler. Laminate design for optimised in-plane performance and ease of manufacture, Composite structures, 177 (2018) 119-128.

[7] C.B. York. New insights into stiffness matching between standard and double angle-ply laminates. 11th Asian-Australian Conference on Composite Materials, Cairns, Australia (2018)

[8] R. Paradies. Designing quasi-isotropic laminates with respect to bending. Composites Science and Technology, 56 (1996) 461-472.

[9] P. Bartholomew. Ply stacking sequences for laminated plates having in-plane and bending orthotropy, Fibre Science and Technology, 10(4) (1977)239-253.

[10] G. Caprino, I. Crivelli-Visconti. A note on specially orthotropic laminates, Journal of Composite Materials, 16(5) (1982) 395-399.

[11] R.J. Mania, C.B. York. Buckling strength improvements for Fibre Metal Laminates using thin-ply tailoring. Composite Structures, 159 (2017) 424-432

[12] C. B. York. Characterization of non-symmetric forms of fully orthotropic laminates. Journal of Aircraft, 46 (2009) 1114-1125.

[13] C. B. York. A unified approach to the characterization of coupled composite laminates: benchmark configurations and special cases. Journal of Aerospace Engineering, 23(4) (2010) 219-242.

[14] C. B. York. On bending-twisting coupled laminates, Composite Structures, 160 (2017) 887-900

[15] C. B. York C. B. and S.F.M. Almeida. Effect of bending-twisting coupling on the compression and shear buckling strength of infinitely long plates. Composite Structures, 184 (2018) 18-29.

[16] H.S.J. Lee, C.B. York. Compression and shear buckling performance of finite length plates with bending-twisting coupling. Composite Structures, 241 (2020) 112069.

[17] C.B. York. Tapered hygo-thermally curvature-stable laminates with non-standard ply orientations. Composites Part A: Applied Science and Manufacturing, 44 (2013) 140-148.

[18] C.B. York. On tapered warp-free laminates with single-ply terminations. Composites Part A: Applied Science and Manufacturing, 72 (2015) 127-138.

[19] C.B. York, S. F. M. Almeida. Tapered laminate designs for new non-crimp fabric architectures. Composites Part A: Applied Science and Manufacturing, 100, (2017) 150-160.

[20] F.W. Williams, M.S. Anderson, D. Kennedy, R. Butler, G. Aston. User Manual for VICONOPT: An exact analysis and optimum design program covering the buckling and

vibration of prismatic assemblies of flat in-plane loaded, anisotropic plates, with approximations for discrete supports, and transverse stiffeners, NASA-CR-181966 (1990)

[21] M.S. Anderson, W.J. Stroud. PASCO: Structural panel analysis and sizing code, users manual. NASA TM-80182 (1981)

[22] M.S. Anderson M. S. W.J. Stroud. General panel sizing computer code and its application to composite structural panels. AIAA Journal, 17(8) (1979) 892-897.

[23] C. B. York, F.W. Williams, D. Kennedy, R. Butler. A parametric study of optimum designs for benchmark stiffened wing panels. Composites Engineering, 3(7-8) (1993) 619-632.

[24] C.B. York. Buckling analysis and minimum-mass design procedures for composite wing-box structures. Journal of Aircraft, 43(2) (2006) 528-536.

[25] C.B. York. Elastic buckling design curves for isotropic rectangular plates with continuity or elastic edge restraint against rotation. Aeronautical Journal, 104(1034) (2000) 175-182.

[26] S.W. Tsai, H.T. Hahn. Introduction to composite materials. Technomic Publishing Co. Inc., Lancaster (1980)

[27] P.M. Weaver and M. P. Nemeth. Bounds on flexural properties and buckling response for symmetrically laminated composite plates. Journal of Engineering Mechanics 133(11) (2007) 1178-1191.

[28] T. Kubiak. Static and dynamic buckling of thin-walled plate structures, Springer International Publishing, Switzerland (2013).

[29] C. Mittelstedt. Buckling and post-buckling of thin-walled composite laminated beams—A review of engineering analysis methods. Applied Mechanics Review, 72(2) (2020) 020802.

FIGURES

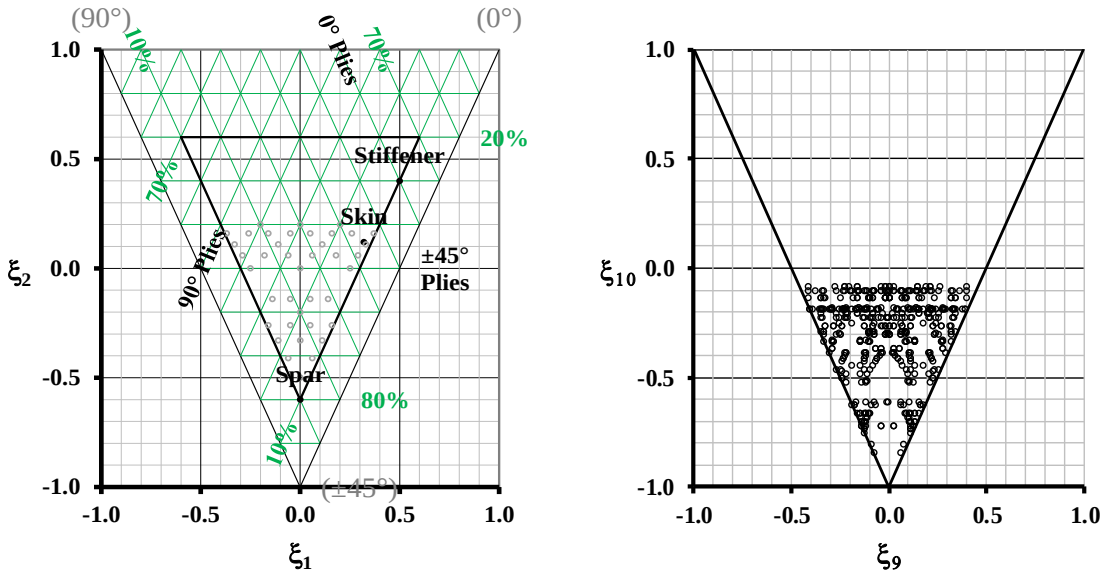

Figure 1 – Lamination parameter design spaces for fully uncoupled symmetric laminates ($12 \leq n \leq 21$ plies), representing: (a) 39 unique coordinate points (ξ_1, ξ_2) in extensional stiffness and (b) the corresponding coordinate points (ξ_9, ξ_{10}) in bending stiffness.

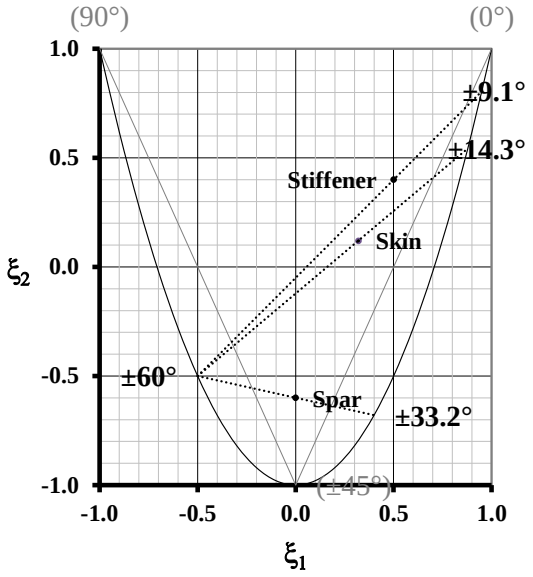

Figure 2 – Hypothetical angle-ply combinations giving matched extensional stiffness to traditional aircraft components, defined by ply percentages in Fig. 1, and represented here as equivalent lamination parameter coorindinates.

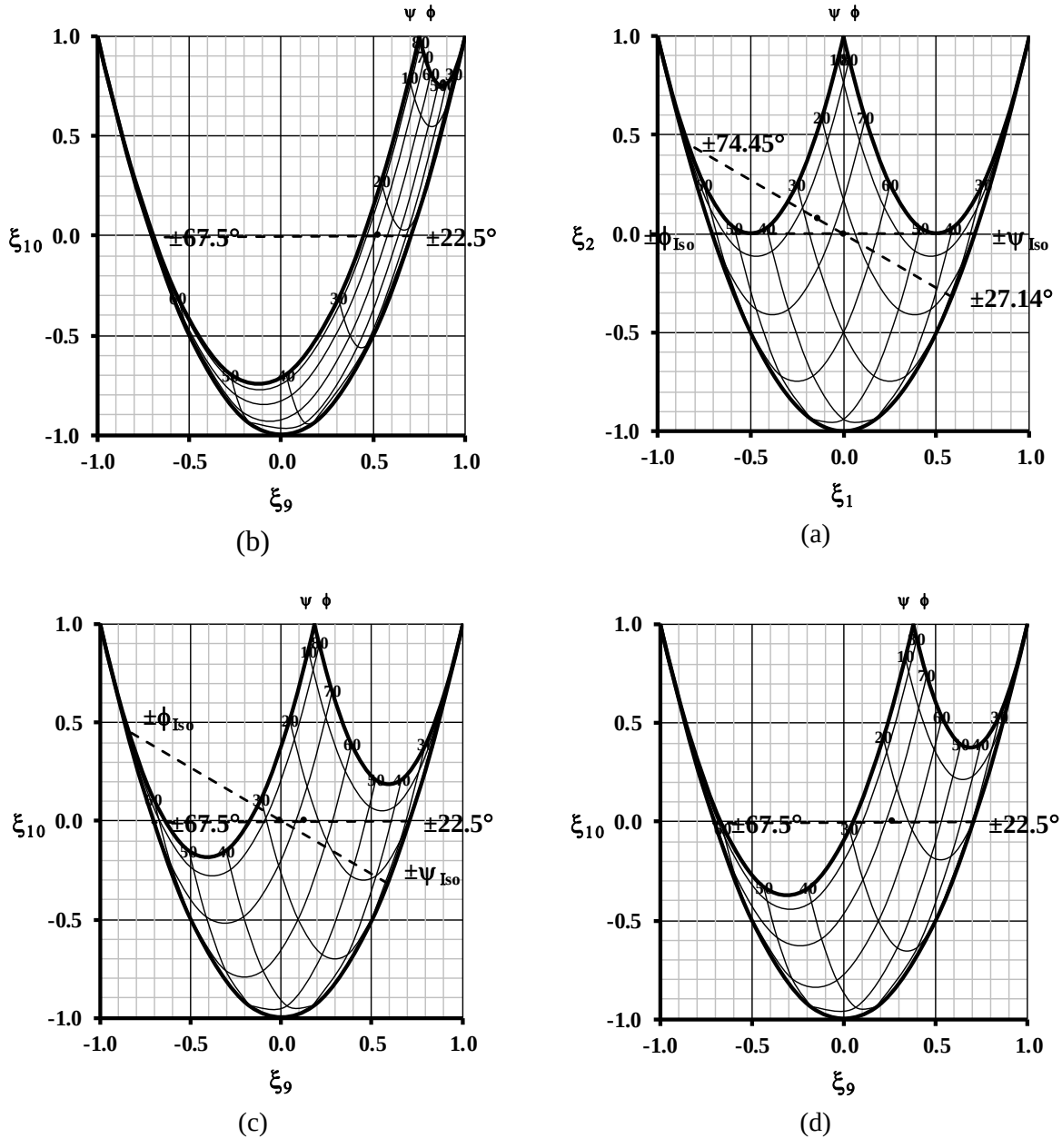

Figure 3 – Lamination parameter design spaces for (a) extensional stiffness for laminates *a* - *f* of Table 7 and; (b) bending stiffness for laminates *a* and *b*; (c) laminates *c* and *d* and; (d) laminates *e* and *f*.

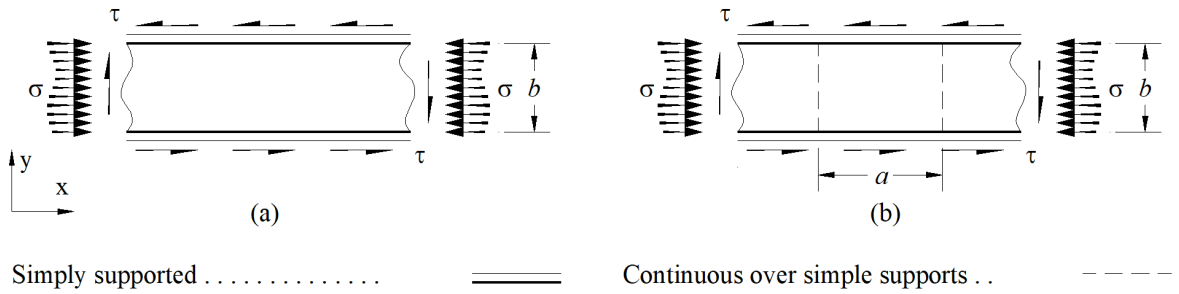

Figure 4 – Infinitely long plates subject to compressive stress, $\sigma = N_x/t$, or shear stress, $\tau = N_{xy}/t$, with (a) simply supported edges and (b) continuity over transverse supports.

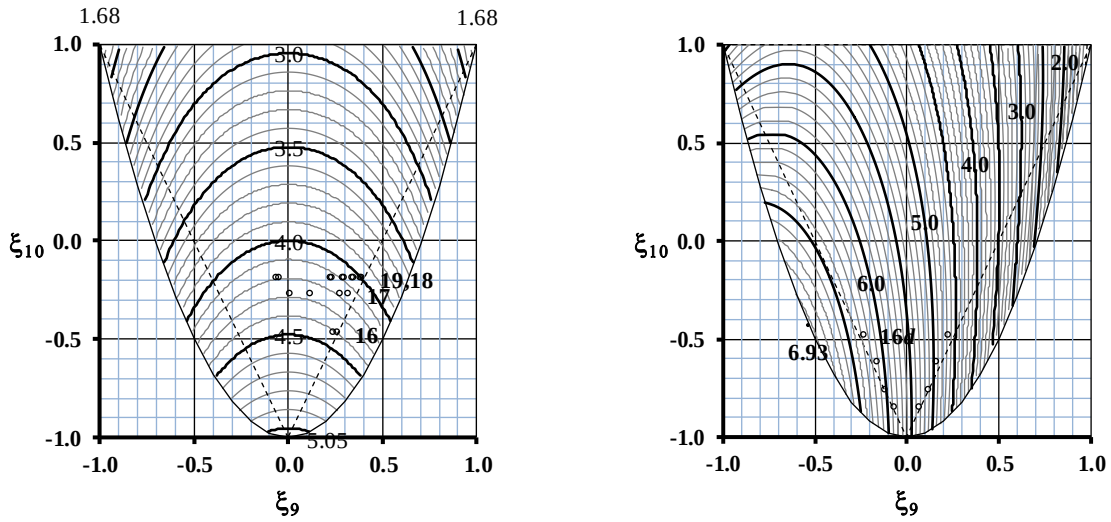

Figure 5 – Buckling contours, superimposed on the lamination parameter design space, for infinitely long plates with simply supported edges in: (a) compression ($k_{x,\infty}$), identifying skin panel designs of Table 3 and (b) Shear ($k_{xy,\infty}$), identifying spar designs of Table 4. The feasible region of lamination parameters for standard-ply designs is indicated by broken lines.

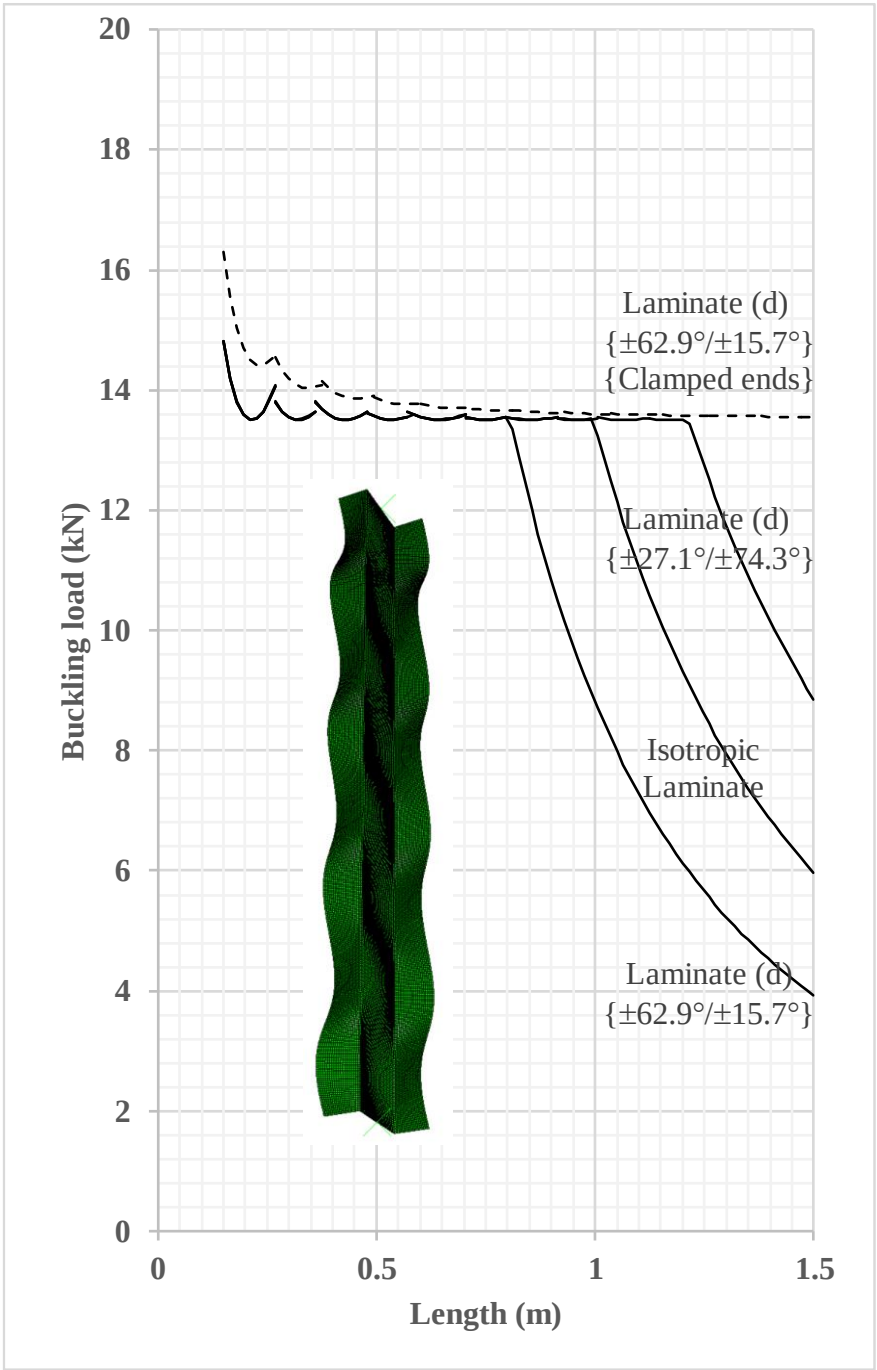

Figure 6: Compression buckling load for Z-section column with simply supported and clamped ends for selected double angle ply laminates, listed in Table 8, with matched Isotropy in bending stiffness using the {±ψ/±ϕ} combinations shown. The local buckling mode shape shown is for the Isotropic laminate with length 800mm.

TABLES

Table 1 – Equivalent isotropic properties, E_{Iso}, G_{Iso} and ν_{Iso} of selected fibre/matrix composite materials for comparison with common Aluminum alloys 2024-T4 (7075-T6), with E = 73.1 (71.7) GPa, G = 28.0 (26.9) GPa and ν = 0.33 (0.33).

Fibre/Matrix material	E_1	E_2	G_{12}	ν_{12}	E_{iso}	G_{iso}	ν_{Iso}
T300/5208 Graphite/Epoxy	181.0	10.3	7.17	0.28	69.7	26.9	0.30
AS/3501 Graphite/Epoxy	138.0	8.96	7.1	0.3	54.8	21.4	0.28
Scotchply 1002 Glass/Epoxy	38.6	8.27	4.14	0.26	19.0	7.47	0.27
Kevlar 49/Epoxy Aramid/Epoxy	76.0	5.5	2.3	0.34	29.0	11.0	0.32
B(4)/5505 Boron/Epoxy	204.0	18.5	5.59	0.23	78.5	29.7	0.32

Table 2 – Example stacking sequences (mid-plane plies denoted by an underscore) for fully uncoupled symmetric Graphite/Epoxy laminates, and associated lamination parameter coordinates in extension (ξ_1, ξ_2) and bending (ξ_9, ξ_{10}), representing the highest possible buckling strength increase above the equivalent isotropic datum, for the case of an infinitely long plate with simply supported edges for: (a) compression, $k_{x,\infty}$, and; (b) shear, $k_{xy,\infty}$. Values in parentheses represent the highest fully uncoupled non-symmetric designs ($k_{x,max,\infty}$) and ($k_{xy,max,\infty}$).

(a)

n	Stacking Sequence	ξ_1	ξ_2	ξ_9	ξ_{10}	$k_{x,\infty}$ ($k_{x,max,\infty}$)
16	$[45/-45/-45/45/0/-45/45/90]_S$	0.00	-0.50	0.07	-0.85	22.14% (24.13%)
12	$[45/-45/-45/90/45/0]_S$	0.00	-0.33	-0.08	-0.81	21.10% (24.25%)
18	$[45/-45/-45/45/90/0/45/-45/0]_S$	0.11	-0.33	-0.03	-0.73	19.70% (22.92%)
17	$[45/-45/-45/90/45/45/-45/0/\underline{0}]_S$	0.06	-0.41	-0.12	-0.74	19.00% (23.55%)
19	$[45/-45/-45/90/45/45/-45/0/0/90]_S$	0.05	-0.26	-0.11	-0.71	18.21% (22.26%)
19	$[45/-45/-45/0/45/45/-45/90/0/\underline{0}]_S$	0.16	-0.26	0.12	-0.71	18.15% (22.24%)
20	$[45/-45/-45/90/45/45/-45/0/0/90]_S$	0.00	-0.20	-0.10	-0.69	17.76% (21.61%)
21	$[45/-45/-45/90/45/45/-45/0/0/0/\underline{90}]_S$	*0.14*	*-0.14*	-0.09	-0.67	17.31% (20.84%)
21	$[45/-45/-45/0/45/45/-45/0/90/90/\underline{0}]_S$	0.05	-0.14	-0.10	-0.67	17.28% (20.87%)
14	$[45/-45/0/-45/90/0/45]_S$	*0.14*	*-0.14*	0.14	-0.49	12.56% (22.04%)
16	$[45/-45/0/-45/90/45/90/0]_S$	0.00	0.00	0.09	-0.47	11.99% (19.67%)
16	$[45/-45/0/-45/0/45/90/0]_S$	0.25	0.00	0.24	-0.47	10.30% (19.31%)
17	$[45/-45/90/0/-45/0/0/45/\underline{90}]_S$	0.18	0.06	0.01	-0.27	7.17% (18.44%)
17	$[45/-45/90/0/-45/0/0/45/\underline{0}]_S$	0.29	0.06	0.01	-0.27	7.16% (18.04%)
17	$[45/-45/90/0/-45/0/90/45/\underline{0}]_S$	0.06	0.06	-0.03	-0.27	7.14% (18.44%)
20	$[45/-45/90/0/-45/0/45/90/90/0]_S$	0.00	0.20	-0.01	-0.23	6.08% (14.90%)
20	$[45/-45/90/0/-45/0/45/90/0/0]_S$	0.20	0.20	0.03	-0.23	6.05% (14.88%)
19	$[45/0/-45/-45/0/0/0/45/90/\underline{0}]_S$	0.37	0.16	-0.04	-0.19	4.97% (15.06%)
19	$[45/0/-45/-45/0/0/0/45/90/\underline{90}]_S$	0.26	0.16	-0.04	-0.19	4.97% (15.91%)
19	$[45/90/-45/-45/0/0/0/45/90/\underline{0}]_S$	0.16	0.16	-0.05	-0.19	4.97% (16.04%)
19	$[45/90/-45/-45/0/0/0/45/90/\underline{90}]_S$	0.05	0.16	-0.05	-0.19	4.95% (16.05%)
18	$[45/90/-45/-45/0/0/0/90/45]_S$	0.11	0.11	-0.08	-0.20	4.93% (17.23%)
18	$[45/0/-45/-45/90/0/0/0/45]_S$	0.33	0.11	0.23	-0.20	3.35% (16.38%)

(b)

n	Stacking Sequence	ξ_1	ξ_2	ξ_9	ξ_{10}	$k_{xy,\infty}$ ($k_{xy,max,\infty}$)
19	$[45/90/-45/-45/90/90/90/45/0/\underline{90}]_S$	-0.37	0.16	-0.40	-0.19	21.00% (21.15%)
19	$[45/90/-45/-45/90/90/90/45/0/\underline{0}]_S$	-0.26	0.16	-0.40	-0.19	20.99% (21.14%)
21	$[45/90/90/-45/-45/-45/90/45/0/45/\underline{0}]_S$	-0.14	-0.14	-0.41	-0.14	20.63% (21.24%)
18	$[45/90/-45/-45/90/90/90/0/45]_S$	-0.33	0.11	-0.38	-0.20	20.53% (21.32%)
20	$[45/-45/90/90/90/-45/90/0/45/0]_S$	-0.20	0.20	-0.40	-0.11	20.01% (20.01%)
21	$[45/90/-45/90/-45/-45/45/45/0/0/\underline{90}]_S$	-0.05	-0.14	-0.32	-0.30	19.54% (19.57%)
17	$[45/-45/90/90/-45/90/0/45/\underline{90}]_S$	-0.29	0.06	-0.32	-0.27	19.18% (20.94%)
17	$[45/-45/90/90/-45/90/0/45/\underline{0}]_S$	-0.18	0.06	-0.32	-0.27	19.16% (20.93%)
16	$[45/-45/90/-45/90/45/90/0/]_S$	-0.25	0.00	-0.26	-0.47	18.68% (21.16%)
19	$[45/-45/90/90/-45/45/-45/0/45/\underline{90}]_S$	-0.16	-0.26	-0.28	-0.38	18.68% (20.45%)
19	$[45/-45/90/90/-45/45/-45/0/45/\underline{0}]_S$	-0.05	-0.26	-0.28	-0.38	18.67% (20.43%)
19	$[45/90/-45/-45/90/90/0/45/0/\underline{90}]_S$	-0.16	0.16	-0.33	-0.19	18.43% (20.05%)
19	$[45/90/-45/-45/90/90/0/45/0/\underline{0}]_S$	-0.05	0.16	-0.33	-0.19	18.42% (18.99%)
18	$[45/90/-45/-45/90/90/0/0/45]_S$	-0.11	0.11	-0.33	-0.20	18.40% (19.56%)
20	$[45/90/-45/-45/90/45/-45/0/0/45]_S$	0.00	-0.20	-0.28	-0.33	18.06% (19.74%)
17	$[45/90/-45/-45/-45/45/45/0/\underline{90}]_S$	-0.06	-0.41	-0.23	-0.51	17.72% (17.72%)
16	$[45/90/-45/-45/-45/45/0/45]_S$	0.00	-0.50	-0.23	-0.48	17.36% (18.22%)
20	$[45/-45/90/90/90/-45/0/0/45/0]_S$	0.00	0.20	-0.33	-0.11	17.14% (17.51%)
18	$[45/-45/90/-45/45/90/-45/0/45]_S$	-0.11	-0.33	-0.22	-0.53	16.89% (21.26%)
14	$[45/-45/90/-45/90/0/45]_S$	-0.14	-0.14	-0.21	-0.49	16.38% (20.04%)
17	$[45/-45/90/90/-45/0/0/45/\underline{90}]_S$	-0.06	0.06	-0.23	-0.27	15.08% (18.34%)
12	$[45/-45/-45/90/45/0]_S$	0.00	-0.33	-0.08	-0.81	10.82% (16.98%)
16	$[45/-45/90/-45/0/45/90/0]_S$	0.00	0.00	-0.12	-0.47	10.81% (18.17%)

Table 3: Initial buckling load increases (%) above isotropic datum for symmetric Graphite/Epoxy laminates most closely matching typical skin panel properties, (ξ_1, ξ_2) ≈ (0.32, 0.16), for the infinitely long plate within each ply number grouping, *n*.

n	Stacking Sequence	(ξ_1, ξ_2)	(ξ_9, ξ_{10})	$k_{x,\infty}$
16	*a*: $[45/-45/0/-45/0/45/90/0]_S$	(0.25, 0.00)	(0.24, -0.47)	10.3%
	b: $[45/-45/0/-45/0/45/0/90]_S$		(0.26, -0.47)	9.9%
17	$[45/-45/90/0/-45/0/0/45/\underline{0}]_S$	(0.29, 0.06)	(0.01, -0.27)	7.2%
	$[45/-45/0/90/-45/0/0/45/\underline{0}]_S$		(0.12, -0.27)	6.7%
	$[45/-45/0/0/-45/90/0/45/\underline{0}]_S$		(0.27, -0.27)	4.6%
	$[45/-45/0/0/-45/0/90/45/\underline{0}]_S$		(0.32, -0.27)	3.6%
18	$[45/0/-45/-45/90/0/0/0/45]_S$	(0.33, 0.11)	(0.23, -0.20)	3.3%
	$[45/0/-45/-45/0/90/0/0/45]_S$		(0.30, -0.20)	2.2%
	$[45/0/-45/-45/0/0/90/0/45]_S$		(0.35, -0.20)	1.1%
	$[45/0/-45/-45/0/0/0/90/45]_S$		0.38, -0.20)	0.2%
19	$[45/90/-45/-45/0/0/0/45/0/\underline{0}]_S$	(0.37, 0.16)	(-0.04, -0.19)	3.3%
	$[45/0/-45/-45/90/0/0/45/0/\underline{0}]_S$		(0.23, -0.19)	2.2%
	$[45/0/-45/-45/0/90/0/45/0/\underline{0}]_S$		(0.29, -0.19)	1.2%
	$[45/0/-45/-45/0/0/90/45/0/\underline{0}]_S$		(0.34, -0.19)	-0.2%
	$[45/0/-45/-45/0/0/0/45/90/\underline{0}]_S$		(0.40, -0.19)	5.0%

Table 4: ·Initial compression ($k_{x,\infty}$) and shear ($k_{xy,\infty}$) buckling load increases (%) above isotropic datum for symmetric Graphite/Epoxy laminates with (ξ_1, ξ_2) = (0.00, -0.50), which most closely match typical Spar properties, (ξ_1, ξ_2) ≈ (0.00, -0.60), for the infinitely long plate.

n	Stacking Sequence	(ξ_9, ξ_{10})	$k_{x,\infty}$	$k_{xy,\infty}$
16	*a*(1): $[45/-45/90/-45/45/-45/0/45]_S$	(-0.16, -0.62)	15.2%	14.7%
	a(2): $[45/-45/0/-45/45/-45/90/45]_S$	(0.16, -0.62)		-7.7%
	b(1): $[45/-45/-45/45/90/-45/45/0]_S$	(-0.07, -0.85)	22.1%	10.1%
	b(2): $[45/-45/-45/45/0/-45/45/90]_S$	(0.07, -0.85)		-0.4%
	c(1): $[45/-45/-45/90/45/45/-45/0]_S$	(-0.12, -0.76)	19.4%	12.8%
	c(2): $[45/-45/-45/0/45/45/-45/90]_S$	(0.12, -0.76)		-4.1%
	d(1): $[45/90/-45/-45/-45/45/0/45]_S$	(-0.23, -0.48)	10.6%	17.4%
	d(2): $[45/0/-45/-45/-45/45/90/45]_S$	(0.23, -0.48)		-13.3%

Table 5: Calculation procedure for the non-dimensional parameters for an uncoupled laminate.

			A					**B**					**D**				
Ply	θ	$(z_k - z_{k-1})$	$A\Sigma_+$	$A\Sigma_-$	$A\Sigma_\bigcirc$	$A\Sigma_\bullet$	$(z_k^2 - z_{k-1}^2)$	$B\Sigma_+$	$B\Sigma_-$	$B\Sigma_\bigcirc$	$B\Sigma_\bullet$	$(z_k^3 - z_{k-1}^3)$	$D\Sigma_+$	$D\Sigma_-$	$D\Sigma_\bigcirc$	$D\Sigma_\bullet$
			4	4	4	4		0	0	0	0		268	268	244	244
1	+	1	→ 1				-15	→ -15				169	→ 169			
2	○	1	→		1		-13	→		-13		127	→		127	
3	●	1	→			1	-11	→			-11	91	→			91
4	–	1	→	1			-9	→	-9			61	→	61		
5	–	1	→	1			-7	→	-7			37	→	37		
6	●	1	→			1	-5	→			-5	19	→			19
7	○	1	→		1		-3	→		-3		7	→		7	
8	+	1	→ 1				-1	→ -1				1	→ 1			
9	–	1	→	1			1	→	1			1	→	1		
10	●	1	→			1	3	→			3	7	→			7
11	○	1	→		1		5	→		5		19	→		19	
12	+	1	→ 1				7	→ 7				37	→ 37			
13	+	1	→ 1				9	→ 9				61	→ 61			
14	○	1	→		1		11	→		11		91	→		91	
15	●	1	→			1	13	→			13	127	→			127
16	–	1	→	1			15	→	15			169	→	169		

Table 6 - Number of double angle-ply solutions for *Uncoupled* and *Bending-Twisting* coupled designs with increasing ply number grouping, *n*, for non-crimp fabrics (NCF) and uni-directional (UD) designs

n =	12	14	16	18	20	22	24
Uncoupled UD			14		110		2,173
Uncoupled NCF			6				108
Bending-Twisting coupled NCF	18		146		1,430		14,134

Table 7: Stacking sequences for fully uncoupled double angle-ply laminates with 16 layers. Bending stiffness proportions ($\zeta_{\pm\phi}/\zeta$) and ($\zeta_{\pm\psi}/\zeta$) are given together with angles (ϕ_{Iso}, ψ_{Iso}) for designs that lead to bending isotropy; (ϕ_{Iso}, ψ_{Iso}) = (62.95°, 15.74°) if ϕ/ψ are switched. Ply proportions ($n_{\pm\phi}/n$) = ($n_{\pm\psi}/n$) = 0.5 for all designs and give Extensional isotropy for (ϕ_{Iso}, ψ_{Iso}) = (67.5°, 22.5°).

Ref.	Stacking sequence	($\zeta_{\pm\phi}/\zeta$)	($\zeta_{\pm\psi}/\zeta$)	ϕ_{Iso}	ψ_{Iso}
a, b	$[\underline{\psi/-\psi/\psi/-\phi/\phi/\phi/-\phi}]_A$, $[\underline{\psi/-\psi/-\psi/\psi/\phi/-\phi/-\phi/\phi}]_A$	0.12	0.88	-	-
c, d	$[\underline{\psi/-\psi/\phi/-\phi/-\phi/\phi/-\psi/\psi}]_A$, $[\underline{\psi/-\psi/-\phi/\phi/\phi/-\phi/-\psi/\psi}]_A$	0.40	0.60	74.45°	27.14°
e, f	$[\underline{\psi/-\psi/\phi/-\phi/-\psi/\psi/-\phi/\phi}]_A$, $[\underline{\psi/-\psi/-\phi/\phi/-\psi/\psi/\phi/-\phi}]_A$	0.31	0.69	-	-

Table 8: Example stacking sequences from the 15 fully uncoupled double angle-ply laminate with 24 layers with: (a) ply proportions ($n_{\pm\phi}/n$, $n_{\pm\psi}/n$) = (0.67, 0.33) for designs *a* – *e* and; (b) ($n_{\pm\phi}/n$, $n_{\pm\psi}/n$) = (0.33, 0.67) for (b) designs *f* - *o*. Bending stiffness proportions ($\zeta_{\pm\phi}/\zeta$) and ($\zeta_{\pm\psi}/\zeta$) are given together with angles (ϕ_{Iso}, ψ_{Iso}) for designs that lead to bending isotropy.

(a)

	Stacking sequence	$\zeta_{\pm\phi}/\zeta$	$\zeta_{\pm\psi}/\zeta$	ϕ_{Iso}	ψ_{Iso}
a	$[\underline{\psi/-\psi/-\phi/\phi/\phi/-\phi/\phi/-\phi/-\phi/\phi/-\psi/\psi/-\psi/\psi/\phi/-\phi/-\phi/\phi/-\phi/\psi/-\psi}]_T$	0.57	0.43	63.78°	17.44°
b	$[\underline{\psi/-\psi/\phi/-\phi/-\phi/\phi/-\phi/\phi/-\psi/\psi/\phi/-\phi/\phi/-\phi/-\psi/\psi/-\phi/\phi/-\phi/\phi/\phi/-\phi/\psi/-\psi}]_T$	0.55	0.45	65.08°	19.58°
c	$[\underline{\psi/-\psi/-\phi/\phi/\phi/-\phi/-\psi/\psi/\phi/-\phi/-\phi/\phi/\phi/-\phi/\phi/-\psi/\psi/-\phi/\phi/\phi/-\phi/\psi/-\psi}]_T$	0.49	0.51	68.06°	23.04°
d	$[\underline{\psi/-\psi/-\phi/\phi/-\psi/\psi/\phi/-\phi/\phi/-\phi/\phi/-\phi/\phi/-\phi/\phi/-\psi/\psi/\phi/-\phi/\psi/-\psi}]_T$	0.41	0.59	74.28°	27.06°
e	$[\underline{\psi/-\psi/-\psi/\psi/-\phi/\phi/-\phi/\phi/\phi/-\phi/\phi/-\phi/\phi/-\phi/\phi/-\phi/\phi/-\phi/\phi/-\phi/\phi/-\psi/\psi/\psi/-\psi}]_T$	0.30	0.70	-	-

(b)

	Stacking sequence	$\zeta_{\pm\phi}/\zeta$	$\zeta_{\pm\psi}/\zeta$	ϕ_{Iso}	ψ_{Iso}
f	$[\underline{\psi/-\psi/\phi/-\phi/-\phi/\phi/\psi/-\psi/-\psi/\psi/-\psi/\psi/-\psi/\psi/-\psi/\psi/-\psi/-\phi/\phi/\phi/-\phi/\psi/-\psi}]_T$	0.45	0.55	70.46°	24.95°
g	$[\underline{\psi/-\psi/\phi/-\phi/\psi/-\psi/-\phi/\phi/-\psi/\psi/-\psi/\psi/-\psi/\psi/-\phi/\phi/\psi/-\psi/\phi/-\phi/\psi/-\psi}]_T$	0.37	0.63	78.64°	28.59°
h	$[\psi/-\psi/\phi/-\phi/\psi/-\psi/-\psi/\psi/-\phi/\phi/-\psi/\psi/-\psi/\psi/-\phi/\phi/-\psi/\psi/\psi/-\psi/\phi/-\phi/\psi/-\psi]_T$	0.31	0.69	-	-
i	$[\psi/-\psi/\phi/-\phi/\psi/-\psi/-\psi/\psi/-\psi/\psi/-\phi/\phi/-\phi/\phi/-\psi/\psi/-\psi/\psi/\psi/-\psi/\phi/-\phi/\psi/-\psi]_T$	0.29	0.71	-	-
j	$[\psi/-\psi/\psi/-\psi/\phi/-\phi/-\phi/\phi/-\psi/\psi/-\psi/\psi/-\psi/\psi/-\psi/\psi/-\phi/\phi/\phi/-\phi/\psi/-\psi/\psi/-\psi]_T$	0.26	0.74	-	-
k	$[\psi/-\psi/\psi/-\psi/\phi/-\phi/-\psi/\psi/-\phi/\phi/-\psi/\psi/-\psi/\psi/-\phi/\phi/-\psi/\psi/\phi/-\phi/\psi/-\psi/\psi/-\psi]_T$	0.20	0.80	-	-
l	$[\psi/-\psi/\psi/-\psi/\phi/-\phi/-\psi/\psi/-\psi/\psi/-\phi/\phi/-\phi/\phi/-\psi/\psi/-\psi/\psi/\phi/-\phi/\psi/-\psi/\psi/-\psi]_T$	0.18	0.82	-	-
m	$[\psi/-\psi/\psi/-\psi/-\psi/\psi/-\phi/\phi/\phi/-\phi/-\psi/\psi/-\psi/\psi/\phi/-\phi/-\phi/\phi/-\psi/\psi/\psi/-\psi/\psi/-\psi]_T$	0.12	0.88	-	-
n	$[\psi/-\psi/\psi/-\psi/-\psi/\psi/-\phi/\phi/-\psi/\psi/\phi/-\phi/\phi/-\phi/-\psi/\psi/-\phi/\phi/-\psi/\psi/\psi/-\psi/\psi/-\psi]_T$	0.09	0.91	-	-
o	$[\psi/-\psi/\psi/-\psi/-\psi/\psi/-\psi/\psi/-\phi/\phi/\phi/-\phi/\phi/-\phi/-\phi/\phi/-\psi/\psi/-\psi/\psi/\psi/-\psi/\psi/-\psi]_T$	0.04	0.96	-	-